AIAA-2003-3652

Sheath in the Presence of Secondary Electron Emission and Sputtering Yield

B. P. Pandey and Subrata Roy
Computational Plasma Dynamics Laboratory
Kettering University, Flint, MI

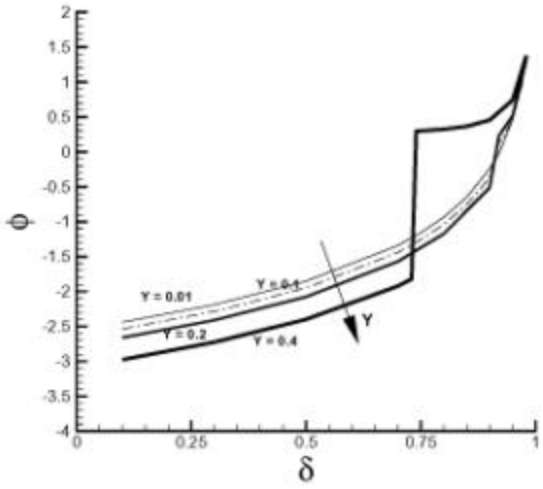

36th AIAA Thermophysics Conference
23-26 June 2003
Orlando, Florida

Sheath in the Presence of Secondary Electron Emission and Sputtering Yield

B.P. Pandey[§] and Subrata Roy[*]

Computational Plasma Dynamics Research Laboratory
Kettering University, Flint, MI 48504

The effect of the secondary electron emission (SEE) and the sputter yield on the plasma dynamics is investigated for two different systems. The analytical formulation is given for one-dimensional, two-fluid unmagnetized plasma. The numerical simulation utilizes multi-fluid description in the presence of external electric and magnetic fields. As the ion sputter yield increases, the analytical result suggest that the saturation of the potential occurs at a smaller value of secondary electron emission coefficient than is possible otherwise. The sheath wall potential and ion energy at the plasma sheath boundary provides the upper limit to the secondary electron emission and sputter yield coefficients. The numerical results show that both SEE and the ion sputter yield alter the plasma characteristics. The plasma number density and temperature decrease in the presence of the SEE while the ion velocity marginally increases. Contrarily, in the presence of the sputter yield, plasma number density and temperature increases whereas, plasma velocity varies all along the channel with about 15% decrease. The potential drop increases in the presence of SEE. However, the neutral number density does not exhibit any significant change.

INTRODUCTION

Sheath formation at the plasma-wall interface is ubiquitous. In bounded plasmas, the Debye length gives the approximate thickness of the sheath, which develops over the inverse electron plasma frequency time scale, whenever plasma is in contact with the material wall. Owing to the large mobility of the electrons, in the absence of such a charged boundary layer, plasma will lose electrons much more rapidly to the wall than the less mobile ions, resulting in a large electric field (current) in the plasma. The charged boundary layer near the wall is a manifestation of the plasma to remain charge neutral. Therefore, in the presence of a stationary sheath, most of the electrons reaching the sheath boundary will be reflected back into the plasma, and number striking the wall will be equal to the number of positive ions reaching the wall. A stationary sheath exists only if the ion flow velocity satisfies the Bohm criteria at the plasma-sheath boundary, or if the electric field at the plasma-sheath interface exceeds some critical value.[1-3]

The problem of sheath dynamics with the plasma-wall interactions is of great importance in a number of areas viz. plasma ion implantation, high-density computer chip development, diamond like film deposition, electric propulsion, nuclear fusion etc. In plasma processing, where a target object is immersed in plasma and pulsed repeatedly to a large negative voltage a sheath is

[§] Post-doctoral Research Fellow, E-mail: bpandey@kettering.edu
[*] Associate Professor, Department of Mechanical Engineering, E-mail: sroy@kettering.edu, Associate Fellow, AIAA

formed that expands into the ambient plasma. If the ion impact energy is sufficiently large, the impact ions may cause severe sputtering of the target, which is an undesirable side effect. The wall may develop the non-uniformities due to sputtering, re-deposition, cracking, etc. Further, sputtered material may contaminate the plasma. Also, the secondary electron emission (SEE) is an important issue. Since the ions and electrons have opposite charge, the emitted secondary electrons are accelerated away from target in the same electric field that accelerates the ions towards the target. This leads to considerable power loss since part of the power goes into the electrons.[4-5] Understanding sheath dynamics is also important in electric propulsion devices. Wall effects can significantly alter the dielectric wall characteristics of Hall thrusters, while impact of high-energy ions may deteriorate the performance of electrodes in MPD thrusters. The design of the future nuclear device must deal with the problem of sputtered wall material. Sputtered wall material, for example, may be ionized in the scrape-off layer and possibly transported into the core plasma, or may be redeposit immediately if the ionization occurs inside the sheath.

Most of the commonly used plasma confining materials have SEE coefficients near or above 0.9 at moderate plasma temperature. For example, boron (15 eV), carbon (12 eV), aluminum (47 eV) etc. have SEE which can reach up to 0.9 .[6] The effect of the cold SEE on the sheath has shown to reduce the sheath potential significantly.[7] In fact the onset of space-charge saturation when the electric field is reversed near the wall surface, has been found to take place within the plasma sheath when SEE coefficient is ~ 0.9.[8] Earlier experimental studies of the effect of SEE on plasma sheath potential showed that the cold electron emission affect bulk plasma properties.[9-10]

The purpose of this study is to find out the relative role SEE and sputter yield (SY) may play in the sheath region. It is shown that both SEE and SY affect the plasma potential and alters Bohm's criteria. We develop an analytical model along the line of Hobbs and Wesson [11] and include the effect of SEE and SY. The result reduces to Hobbs and Wesson's[11] in the absence of sputtering yield. Numerical study is based on the 1D finite element model of Roy and Pandey[12] where the effect of sputtering yield and secondary emission on the dynamics was investigated in the presence of positive wall potential. However, very often, the potential at the dielectric wall is negative and therefore, the 1D wall interaction model[12] needs to be generalized. Further, the paper presents the isolated effect of the secondary electron emission and the sputtering yield on the plasma dynamics.

ANALYTICAL MODEL

We shall assume a collisionless sheath model and employ two-fluid description. Due to the formation of the sheath near the plasma boundary, there exists two regions in a bounded plasma: (a) The quasi-neutral bulk plasma, where electron and ion number densities equal each other and (b) the sheath at the boundary, where electron number density is much less than the ion number density.

Let us consider an infinite plane wall, located at $z = 0$, in contact with the plasma filling the half space $z > 0$. Further, we assume that the sheath-presheath boundary is located at $z = z_0$. The typical sheath width is a few Debye length (a spatial scale of local electric field) that could be very small in practical applications, while the quasi-neutrality scale corresponds to the typical size of the system. These circumstances lead to non-universality of the plasma distribution functions for the whole region and allow the near wall sheath layer to be modeled separately from the bulk plasma region.[2] Let n_{e1}, n_{e2} denote the number density of the primary and secondary electrons and n_{i1}, n_{i2} denote the number densities of the primary and sputtered ions. We shall assume that the sputtered matters are all ionized. At $z = \infty$, far from the wall, plasma is quasi-neutral.

$$n_{e1}(\infty) + n_{e2}(\infty) = n_{i1}(\infty) + n_{i2}(\infty) = n_0 \qquad (1)$$

If the electrons are in thermal equilibrium at $z = \infty$ then the primary electron density in the sheath region can be given as

$$n_{e1} = \left[n_0 - n_{e2}(\infty)\right]\exp\left(\frac{ej}{T}\right) \qquad (2)$$

where $j(z)$ is the sheath voltage and $\varphi(\infty)=0$ and n_0 is the plasma number density when $\varphi(\infty)=0$, and T is the electron energy in eV with e as the electron charge.

The secondary electrons emit from the wall and then fall freely through the sheath. Since secondary electrons have negligible energy (compared to the primary), their energy is ignored. From the continuity

equation, one may write for the secondary electron flux, $J_{e2} \equiv n_{e2}(z)V_{e2}(z) = \text{Constant}$, where $V_{e2}(z)$ is the velocity of the emitted secondaries. From the momentum equation, for velocity

$$\frac{mV_{e2}^2}{2} - e\,j(z) = -e\,j(0) \qquad (3)$$

Here m is electron mass. If δ denotes the number of secondaries emitted per primary from the wall, then

$$n_{e2}(z)V_{e2}(z) = \delta\, n_{e1}(z)V_{e1}(z) \qquad (4)$$

The ions of mass M are assumed cold ($T_i=0$). The ions arrive at the plasma sheath boundary with kinetic energy $E_0 = M V_0^2/2$,and then fall freely into the wall in the presence of the potential field j (z). Thus, for ions,

$$ej(z) + \frac{MV_{i1}^2}{2} = \frac{MV_{i0}^2}{2}. \qquad (5)$$

Then

$$V_{i1} = \sqrt{\frac{2}{M}(E_0 - ej)} \qquad (6)$$

The sputtered material from the wall contains both neutral as well as positively charged ions. Neutrals may get ionized inside the sheath and move towards the wall. As noted above, we shall assume that the sputtered material is completely ionized with the same mass and charge as of the incoming primary ions. Then the density of the sputtered ion is given by conservation of flux, $J_{i2} \equiv n_{i2}(z)V_{i2}(z) = \text{Constant}$ and

$$ej(z) + \frac{MV_{i2}^2}{2} = -ej(0). \qquad (7)$$

Here onwards, the wall potential, $j(0)=j_W$. If Y denotes the number of sputtered ions per primary, then

$$n_{i2}(z)V_{i2}(z) = Yn_{i1}(z)V_{i1}(z) \qquad (8)$$

Now balancing the flux at the plasma-sheath boundary yields

$$J_{i1} - J_{i2} = J_{e1} - J_{e2} = n_0 V_0(z) \qquad (9)$$

Here fluxes $J_{i1}=n_{i1}V_{i1}$ and $J_{e1}=n_{e1}V_{e1}$. From Eqs. (4) and (9) one gets,

$$J_{e1} = \frac{1}{1-\delta} n_0 V_0(z), \quad J_{e2} = \frac{\delta}{1-\delta} n_0 V_0(z) \quad (10)$$

and, from Eqs. (8) and (9),

$$J_{i1} = \frac{1}{1-Y} n_0 V_0(z), \quad J_{e2} = \frac{Y}{1-Y} n_0 V_0(z) \qquad (11)$$

Making use of Eqs. (3), (7) and (9), one may write n_{e2} as

$$n_{e2} = n_0 \left(\frac{\delta}{1-\delta}\right)\left(\frac{m}{M}\frac{E_0}{e(j-j_W)}\right)^{0.5} \qquad (12)$$

From Eqs. (1) and (3),

$$n_{e1} = n_0 \left[1 - \left(\frac{\delta}{1-\delta}\right)\left(\frac{-m}{M}\frac{E_0}{ej_W}\right)^{0.5}\right]\exp\left(\frac{ej}{T}\right) \qquad (13)$$

The Poisson's Eqn. (PE) becomes

$$e_0\nabla^2 j = en_0 \left[\begin{array}{l} \left[1 - \left(\frac{\delta}{1-\delta}\right)\left(\frac{-m}{M}\frac{E_0}{ej_W}\right)^{0.5}\right]\exp\left(\frac{ej}{T}\right) \\ + \left[\left(\frac{\delta}{1-\delta}\right)\left(\frac{m}{M}\frac{E_0}{e(j-j_W)}\right)^{0.5}\right] - \\ \left[1 - \left(\frac{Y}{1-Y}\right)\left(\frac{-E_0}{ej_W}\right)^{0.5}\left(\frac{1}{1-ej/E_0}\right)^{0.5}\right] \\ -\left(\frac{Y}{1-Y}\right)\left(\frac{-E_0}{e(j+j_W)}\right)^{0.5} \end{array}\right]$$

Near the sheath edge, assuming $ej << T$ and $ej << E_0$, one can expand the term on the right hand side of PE. As a result, PE can be written as,

$$\frac{d^2 j}{dz^2} - \frac{j}{k^2} = 0 \qquad (14)$$

$$k^2 = l_D^2 \left[\begin{array}{l} 1 - \left(\frac{\delta}{1-\delta}\right)\left(\frac{-m}{M}\frac{E_0}{ej_W}\right)^{0.5}\left(1 - \frac{T}{2ej_W}\right) - \\ \frac{T}{2E_0} + 0.5\left(\frac{Y}{1-Y}\right)\left(\frac{-E_0}{ej_W}\right)\left(\frac{T}{E_0} - \frac{T}{ej_W}\right) \end{array}\right]$$

The solution of Eq. (14) with $\varphi(\infty)=0$, is $j = A\exp(-z/k)$ where A is a constant.

Note, in the absence of SEE ($\delta \to 0$) and SY ($Y \to 0$), $\kappa \to \lambda_D$ since $T << 2E_0$ and $E_0 << ej_W$. The solution for $\varphi(z)$ is strictly valid only near the plasma edge of the sheath. If $T >> 2E_0$ then in the absence of SEE and SY, κ would be imaginary and the electric potential would be an oscillating function near the wall. Thus, $T < 2E_0$ must be satisfied for the formation of a stable plasma sheath (the Bohm criteria). From the marginal condition for the plasma sheath formation (denominator of $\kappa^2 > 0$), one gets the following modified Bohm criterion,

$$E_0 = \frac{T}{2} + \frac{d}{1-d}\left(\frac{m}{M}\right)^{0.5}\left(\frac{-E_0}{ej_W}\right)^{1.5}\left(\frac{T}{2} - ej_W\right) + \left(\frac{Y}{1-Y}\right)\left(\frac{-E_0}{ej_W}\right)^{1.5}\frac{T}{2E_0}(E_0 - ej_W) \quad (15)$$

In Y→0 limit, one recovers the result of Hobbs and Wesson.[11] Balancing the particle current on the wall,

$$(1-d)\, n_{e1} V_{eth} = (1-Y)\, n_{u1} C_s \quad (16)$$

with $V_{eth} = \sqrt{\frac{8T}{pm}}$, $C_s = \sqrt{\frac{T}{M}}$, one gets

$$\left(\frac{8T}{pm}\right)^{0.5}\left[1 - \frac{d}{1-d}\left(\frac{-m}{M}\frac{E_0}{ej_W}\right)^{0.5}\right]\exp\left(\frac{ej_W}{T}\right) = \left(\frac{1-Y}{1-d}\right)\left[1 - \frac{Y}{1-Y}\left(\frac{E_0}{ej_W}\right)^{0.5}\right]\left(\frac{m}{M}\right)^{0.5} \quad (17)$$

Neglecting *m/M* term in the numerator, an approximate expression for the wall potential for $E_0 \gg T/2$ can be written as,

$$ej_W \approx -T \ln\left\{\left(\frac{1-d}{1-Y}\right)\frac{\sqrt{M/2pm}}{1 - \frac{Y}{1-Y}\left(\frac{-E_0}{ej_W}\right)^{0.5}}\right\} \quad (18)$$

In the absence of *Y*, the wall potential is identical to Eq. (4) of Hobbs and Wesson.[11] One sees from Eq. (18) that the wall potential is a function of δ and *Y*. The presence of *Y* makes the determination of j_W complicated. Eq. (18) is solved numerically and plotted in Fig. 1 and Fig. 2.

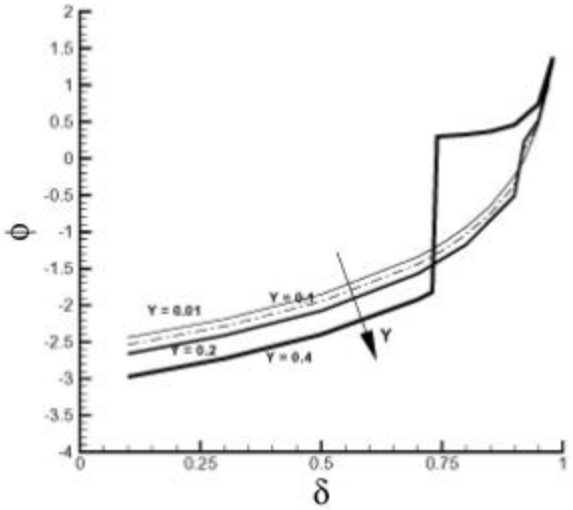

Figure 1. Normalized wall potential vs. SEE for a given sputter yield Y.

The normalized wall potential $f = ej_W/T$ is plotted in Fig.1 against the secondary electron emission δ for different values of sputtering yield, *Y*. One sees that the wall potential saturates with the increasing δ. The saturation of wall potential in the presence of SEE has been noted in many experimental[7-10] as well as theoretical studies.[13-15] From the potential curves for different *Y* one sees that the saturation of the wall potential is a sensitive function of both SEE and SY. For very small value of SY, *Y=0.01*, the potential curve is smooth and transition from negative to positive value is gradual. However, when SY is large, *Y=0.4*, the saturation of the potential is abrupt. This can be anticipated on the ground that ions, which are emitted from the wall find themselves moving towards the wall along with the primary ions that is coming from the bulk plasma and, together, increased ion population reduces the negative wall potential. Further, coupled with the significant emission of cold secondary electrons, the wall potential quickly becomes positive. Therefore, one would expect the sharp saturation of the potential in the presence of both SEE and SY. As a result, one would expect that the saturation of the potential take place at a much smaller SEE. This is confirmed from Fig.1 where saturation for *Y=0.4* takes place at a smaller δ *(< 0.75)* than saturation for *Y=0.2*.

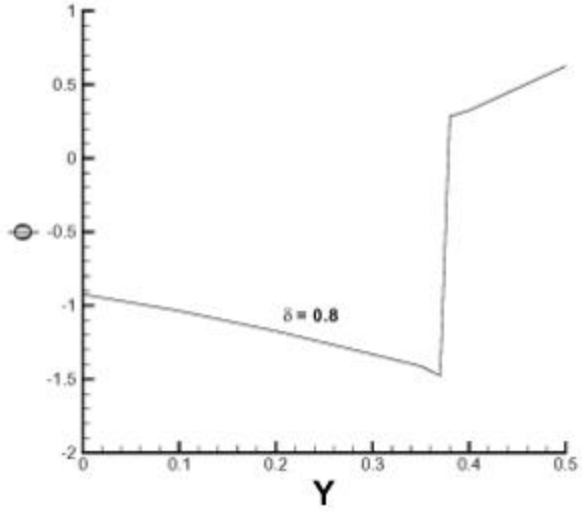

Figure 2. Normalized potential vs. Y for δ = 0.8.

In Fig. 2, wall potential is plotted against SY, *Y* for a given value of SEE (δ = 0.8). The sign change of potential is very rapid. In a very narrow band of *Y*, the potential changes from negative to the positive value.

The shock-like saturation feature displays the sensitivity of the wall potential to the SY. Once a critical value of Y is reached, the wall potential jumps from negative to positive value.

NUMERICAL MODEL

Here we assume a partially ionized plasma, (consisting of electrons, ions and neutral xenon particles), in the presence of external electromagnetic fields. In such a plasma, several important elastic and inelastic processes can take place simultaneously. However, not all processes are equally probable. For example, momentum exchange between electron-electron and ion-ion will not be important in comparison with the electron-ion momentum exchange, as the relative drift between similar particles is small in comparison with the drift between electrons and ions. The plasma is assumed quasi-neutral, i.e. locally the electron number density n_e is equal to the ion number density n_i, as the Debye length is considerably smaller than the width of the physical system. The assumption of quasi-neutrality is valid except near the thin sheath layer. The present work includes the sheath effect by choosing the proper wall boundary conditions and also, by including the plasma-wall interaction terms in the dynamics.

We assume that the ions are unmagnetized. Therefore, the effect of magnetic field on the ion transport will be ignored. The pressure term in the ion momentum equation can be ignored, as the thermal energy of the ion is much smaller than its kinetic energy. Note that owing to the small inertia, electron response time is much faster than the ion response time. As a result, electrons will attain the steady state faster than the ions. Keeping this in mind, electron momentum and energy equations are solved at steady state, whereas for ions and neutrals, a set of time independent continuity and momentum equations are simultaneously solved. It is assumed that the neutral gas flows in the 2D channel (r,z) through the anode hole at the inlet located at (r,0). The plasma is formed inside the channel after impact ionization of the neutral with the incoming electrons to the anode from the cathode located outside the channel (r,L). The plasma is modeled by the 1D, cylindrical (r, q, z) geometry, in the presence of imposed, axial, electric field E_z and radial magnetic field B_r. Following one-dimensional equations are solved in the present work.

Electron momentum equation:

$$V_{ez}\frac{\partial V_{ez}}{\partial z} = -\frac{1}{mn_e}\frac{\partial}{\partial z}(p_e) - \frac{e}{m}E_z - \left(\frac{w_c^2}{n_{ei}+n_{en}+a_B w_c}\right)V_{ez} \qquad (19)$$
$$-n_{ei}(V_{ez}-V_{iz}) - n_{en}(V_{ez}-V_{nz}) - \left(\frac{S}{n_e}\right)(V_{ez}-V_{nz}) + n_w V_{ez}.$$

where n_e is the electron number density. V_{ez}, V_{iz}, V_{nz} are respective electron, ion and neutral axial velocities. $V_\theta = E_z/B_r$ is the azimuthal electron drift velocity, E_z is the axial electric field and B_r radial magnetic field, $p_e = n_e T_e$ is the electron pressure with T_e as the electron temperature in eV, $w_c = eB_r/m$ is the electron-cyclotron frequency, and the source term due to the ionization, recombination and the charge exchange is $S = S_{recomb} + S_{ioniz} + S_{cex.}$ Following relation between azimuthal and axial velocities is utilized,

$$V_{eq} = \left(\frac{w_c}{n_{ei}+n_{en}+a_B w_c}\right)V_{ez} = \Omega V_{ez}. \qquad (20)$$

where α_B is the Bohm diffusion coefficient and Ω is the Hall parameter. We model plasma wall interaction by introducing the electron-wall collision frequency ν_w. Further, the effect of anomalous Bohm conductivity has been included qualitatively by including the equivalent frequency $\nu_B = \alpha_B \omega_c$, that incorporates the effect of magnetic field fluctuations. The Bohm parameter α_B is related to the anomalous diffusion of the electron across the magnetic field. The electron-wall frequency has been modeled by the last term in the equation (19), where ν_w for a channel of width h is given as

$$n_w = \begin{cases} \dfrac{2V_{the}}{h} e^{j'}\left(\dfrac{1-d}{1-Y}\right); & j' \le 0, \\ \dfrac{2V_{the}}{h}; & j' \ge 0. \end{cases} \qquad (21)$$

Here $j' \equiv |e|j_w / T_e$ is the normalized wall potential. Based on the experimental observations, we shall use an empirical formula used for sputter yield,[16]

$$Y = \frac{S}{H_s}(T_i - 4H_s), \qquad (22)$$

where $S = 1\times10^{-2}$ is the sputtering yield factor,[17] H_s = 3000 K is the sublimation energy of channel wall, which is assumed to be made up of ceramic material, boron nitride. The T_i is the incident ion energy on the target. In the present work, we shall assume $T_i = 0.1\ T_e$. The secondary electron emission coefficient for Boron nitride wall is given as,[18]

$$d = \left(\frac{T_e}{E_w} \right)^p . \qquad (23)$$

Here E_w = 16.64 eV for p = 0.576 and E_w = 17.0 eV for p = 0.5.

The dynamics of the electron is determined by the pressure gradient, by the electric and magnetic forces and by the collisional exchange of momentum in equation (19). The convective term in equation (19) retains the effect of the electron inertia. Further, all the collision terms are retained in the electron momentum equation (19).

Neglecting the effect of radiation, viscous dissipation and thermal conduction, electron energy equation can be written as

$$\frac{d}{dz}\left[n_e V_{ez} \left\{ \frac{m(1+\Omega^2)V_{ez}^2}{2} + \frac{5}{2}T_e \right\} \right] - n_e e V_{ez} \frac{dj}{dz} = \qquad (24)$$

$$3\frac{m}{M} n_e n_a (T_i - T_e) + 3\frac{m}{m_h} n_e n_{en} (T_n - T_e) + S\left(\frac{3}{2}T_e + aE_I \right) - n_e n_w E^{'}$$

Here T_e , T_i and T_n (~.3 eV) are electron, ion and neutral temperatures in eV, respectively, and E_I is the ionization energy of the Xenon. Equation (24) includes the effect of the Joule heating, contribution due to the exchange of random thermal energy and due to the ionization and recombination and interaction of the plasma with the wall. The convective flux of the kinetic energy includes the flux of the azimuthal electron kinetic energy $V^2 = V_{ez}^2 + V_{e\theta}^2 = (1+\Omega^2) V_{ez}^2$. The value of α is between[19] (2 –3) and

$$n_w E^{'} = \begin{cases} \frac{2T_e V_{the}}{h} e^{j^{'}} \left[\left(2 - j^{'} \right) - d\left(2\frac{T_{se}}{T_e} - j^{'} \right) \right]; & j^{'} \le 0, \\ \frac{4T_e V_{the}}{h} \left(1 - 2\frac{T_{se}}{T_e} \right); & j^{'} \ge 0. \end{cases} \qquad (25)$$

Here, T_{se} is the temperature of secondary electrons and assumed to be of the order of 0.1 T_e.

Ion continuity:

$$\frac{\partial n_i}{\partial t} + \frac{\partial (n_i V_{iz})}{\partial z} = S - n_w n_i \ , \qquad (26)$$

ion momentum:

$$\frac{\partial V_{iz}}{\partial t} + V_{iz}\frac{\partial V_{iz}}{\partial z} = \left(\frac{e}{M} \right) E_z + \left(\frac{m}{M} \right) n_{ei} (V_{ez} - V_{iz}) \qquad (27)$$

$$- \left(\frac{m_n}{M} \right) n_{in} (V_{iz} - V_{nz}) - \left(\frac{S}{n_e} \right) V_{iz} + n_w V_{iz}$$

and neutral continuity:

$$\frac{\partial n_n}{\partial t} + \frac{\partial (n_n V_{nz})}{\partial z} = -S_n . \qquad (28)$$

Here, $S_n = S_{recomb} + S_{n,ioniz} + S_{cex}$ and $S_{nioniz} = k_i^{0+} n_e n_n + k_i^{0++} n_e n_n$. Equations (19)-(28) are supplemented with the current and mass conservation equations respectively as,

$$e n_i (V_i - V_e) = J_T , \qquad (29)$$

$$m_n n_n V_{nz} + m_i n_i V_{iz} = \frac{\dot{m}}{A}. \qquad (30)$$

Here $J_T = I_d/A$ is the total current density; I_d is the total discharge current, A is the cross section of the channel and $\dot{m}$ is the mass flow rate.

The physical variables are normalized Temperature T_e is normalized to the first ionization potential of Xenon, $T_* = E_I$ = 12.1 eV. Then all dependent variables can be normalized by using their reference values, $V_* = \sqrt{(T_*/m_i)} = 4\times10^3$ m/s, $n_* = \Gamma/V_* = 2.5\times10^{19}$ m^{-3}, and $n_* = s_* \Gamma_*$ s^{-1} where $s_* = s_0\sqrt{(m_i/m_e)}$, $s_0 \cong 3.6\times10^{-20}$ m^2 for Xe. The fundamental length scale can be defined in terms of the characteristic velocity and collisional frequency as, $l_0 = V_*/n_*$. The time scale is $t_0 = n_*^{-1}$.

BOUNDARY CONDITIONS

The numerical model description is incomplete without a set of well-posed boundary condition. Here the 1D radial magnetic field geometry is considered. A shifted Gaussian (bell shaped) magnetic field profile is assumed, which reaches maximum at the exit plane

$$B_r(z) = B_0(z) + B_{\max} \exp(-(z - z_{exit})^2) \qquad (31).$$

At the inlet, the neutral number density is assumed equal to some reference density n_* and the plasma density is fixed $n_i = 0.14 n_*$. The axial ion velocity is not fixed at the inlet. Under typical conditions, next to anode, a plasma sheath (typical width ~ Debye length) forms and ions must flow into the sheath from the quasi-neutral region. The axial velocity is near zero close to the anode and then begins to rise at the edge of the acceleration zone and reaches maximum velocity beyond the exit.[20] Such flow behavior has also been observed in the classical nozzle problem, where flow changes smoothly from subsonic (in the narrow region) to supersonic in the divergent region. Therefore, at the exit the flow velocity should at least attain the characteristic speed of the medium, i.e., the sonic point. In conformity with the available

experimental results and the numerical model,[19] we impose ion velocity at the exit boundary, whereas electron velocity is assumed zero at the inlet. At the inlet, a homogeneous Neumann condition for electrostatic potential is imposed. At the downstream boundary (thruster exit plane), we specify an electron temperature T_e = 10 eV, that is close to the experimental results.[20] At the cathode, a vanishing potential is assumed. For neutral and ion densities along with the electron velocity, a homogeneous Neumann condition is assumed at the exit. The velocity of the neutral is consistently calculated from the mass flow equation.

In the present work, a 1D finite element formulation is used to solve equations (19)-(30). The detailed description of the numerical algorithm is given elsewhere.[12,21] The choice of time step is dictated by the Courant-Fredrich-Levy condition.[22] The code uses variable time steps till the transient features die down as the iteration converges to a steady state. The solution is declared convergent when the maximum residual for each of the state variable becomes smaller than a chosen convergence criterion: $\in = 10^{-4}$.

NUMERICAL RESULTS AND DISCUSSION

Equation set (19)-(30) has been solved over a computational domain (z/L:0,1) where L is the channel length with the exit plane located at 2 cm. The mesh consists of 40 equal length 1-D quadratic finite elements (i.e., 81 nodes) for all numerical results presented here.

The plasma density profiles are given in Fig. 3 and 4. In Fig. 3a, plasma number density is plotted for the values of SEE, δ = 0., 0.80, 0.90 and 0.95 in the absence of sputter yield, Y = 0. The number density (Fig. 3a) increases rapidly from 1.9×10^{17} m^{-3} to 6×10^{18} m^{-3} near the exit plane. We see that the plasma number density remains almost unaffected in the most of the channel except in the acceleration zone. Further, for δ = 0., 0.80, 0.9, the effect of SEE is not significant. However, the effect of SEE becomes pronounced as δ increases, i.e., for δ = 0.95. The inset of Fig. 3a gives an expanded view of the acceleration region where the plasma number density decreases by nearly 7% due to SEE. Similar effects of SEE on the plasma number density have been reported in the literature.[13] The decrease in the number density is consistent with the increase in δ. This is due to the fact that an increase in δ implies an increase in the plasma-wall interaction and hence, the loss of plasma particles. However, the relation between SEE and plasma number density is not a linear one. The increase in the SEE causes the decrease in the plasma temperature since most of the "intermediate-energy" primary electrons will be lost to the wall. This in turn will affect the ionization. As a result, plasma number density will decrease. Subsequently this will lead in the decrease of the secondary electron population itself.

In Fig. 3b, plasma number density is plotted in the absence of the SEE (δ = 0) and, for different values of Y. The effect of Y on plasma density is very pronounced, especially between Y = 0.6 and Y = 0.7. The decline in plasma density is dramatic for Y = 0.7. Recalling that the plasma wall interaction frequency varies as 1/(1 – Y), rapid decline in the number density appears as a result of the plasma-wall frequency becoming very large as Y crosses some critical value. In the present case, such a value is Y = 0.7

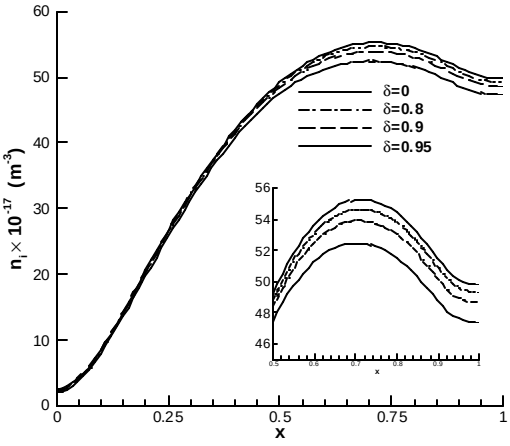

(a)

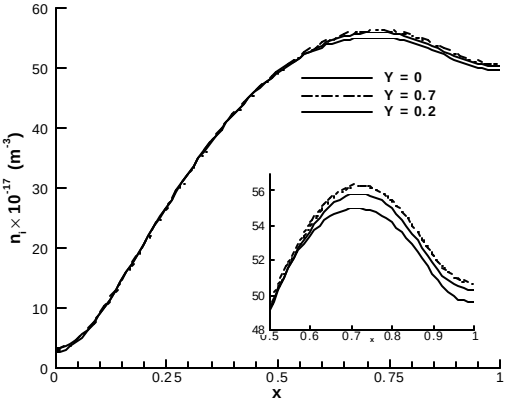

(b)

Figure 3. Normalized plasma density for the different values of secondary electron emission (SEE, δ) and sputter yield Y.

The rapid increase in the ion number density is reflected in the rapid decrease in the neutral number density (Fig. 4a, 4b) from 2.0×10^{19} m^{-3} to approximately 1.55×10^{19} m^{-3}. This is consistent with the fact that as the neutral enters the thruster chamber it undergoes the impact ionization. The SEE (Fig. 4a) and sputter yield Y (Fig. 4b) have no significant effect on the neutral density distribution except near the exit. This result is expected, as there is no direct coupling to the plasma-wall interaction with the neutral dynamics. The change in the neutral density does not exhibit the significant increase downstream of the channel as reported in other work.[13]

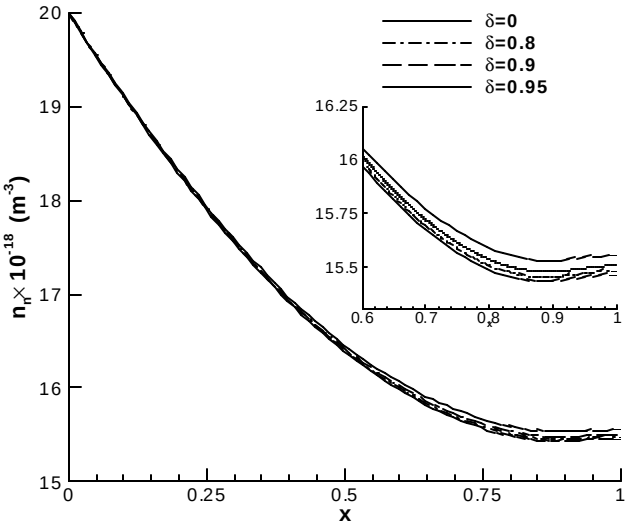

Figure 4(a)

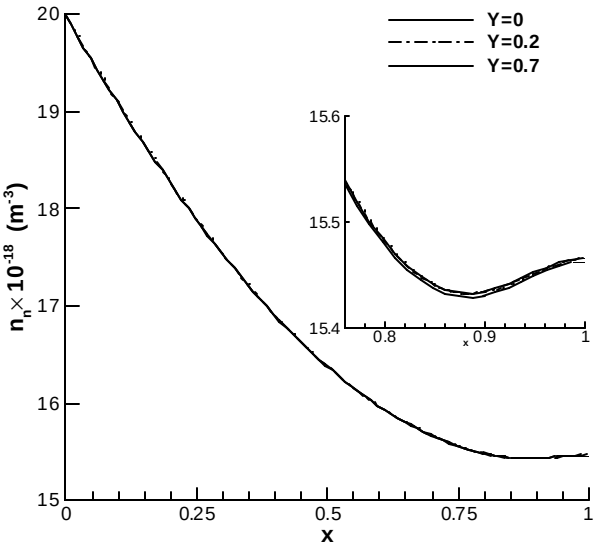

Figure 4(b)

Figure 4. Normalized plasma density for various values of SEE and sputter yield. Curve (a) correspond to δ = 0.8 and Y = 0, curve (b) δ = Y = 0.5 and, curve (c) when SEE and Y, both are calculated self-consistently from the dynamics.

Such a behavior indicates that the sputter yield and secondary electron emission are intimately linked and they affect each other. The increase in the SEE leads to the decrease in the plasma density that in turn leads to the decrease in plasma temperature. The decreased plasma density will have lesser number of energetic ions and hence, a decrease in the sputter yield. The decreased plasma density will reduce the SEE. Therefore, the process of SEE, sputter yield and the process of ionization, recombination will regulate each other before the system reaches the steady state.

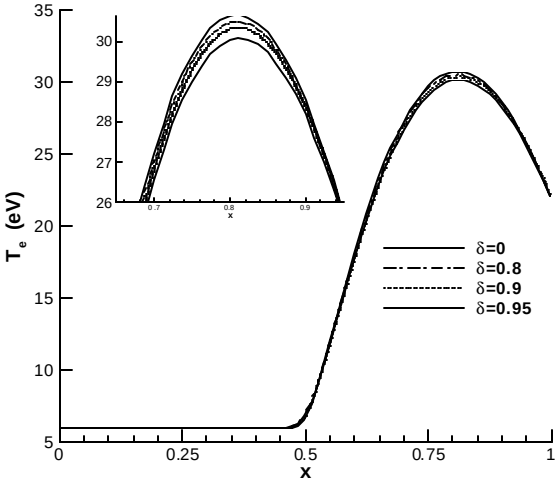

Figure 5(a)

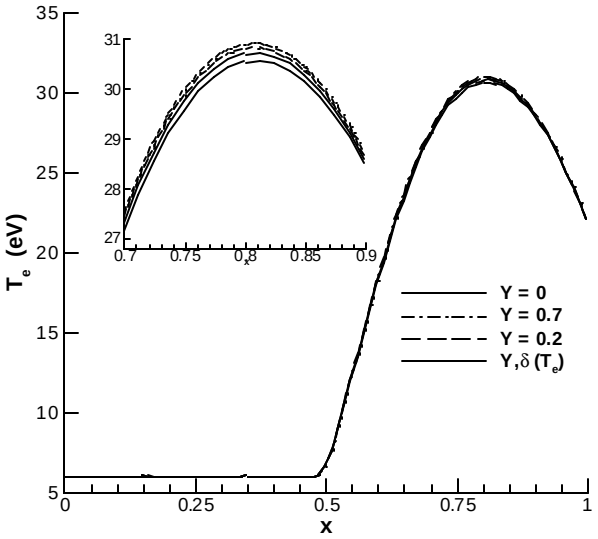

Figure 5(b)

Fig. 5a describes the electron temperature profile for different values of SEE. The increase in the electron temperature is not uniform and the maximum increase occurs just downstream of the center of the channel. The peak in the electron temperature can be attributed to the maximum gyration energy in this region. In the presence of SEE, the electron temperature is slightly lower than in its absence. This result suggests that for a given, fixed SEE, average electron temperature decreases due to the presence of large number of "cold" secondaries. Inset of the figure describes this marginal change.

In Fig. 5b, we first plot the electron temperature in the absence of secondary electron emission with different values of Y. The increase in Y is accompanied with the increase in the electron temperature. With the increase of "cold" ions, the slow and intermediate electrons may be lost due to their recombination with the emitted ions. As a result, the increase in the electron temperature with the increasing Y is indicative of the presence of high thermal electrons. The increase in electron temperature is small when both Y and δ are calculated in a self-consistent temperature dependent manner. The general profile of the temperature remains similar to the previous case.

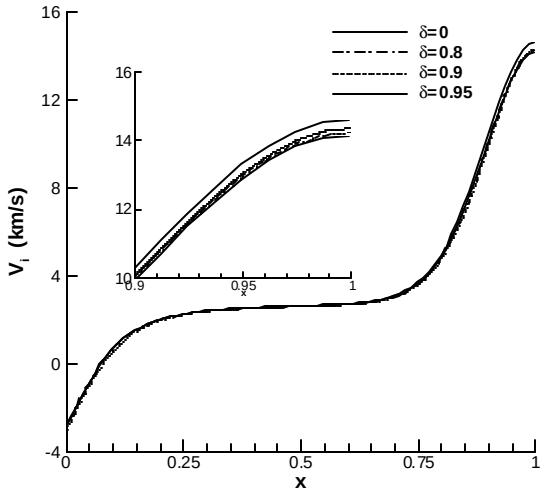

Figure 6a. Ion velocity shows insignificant effect of secondary electron emission δ for Y=0.

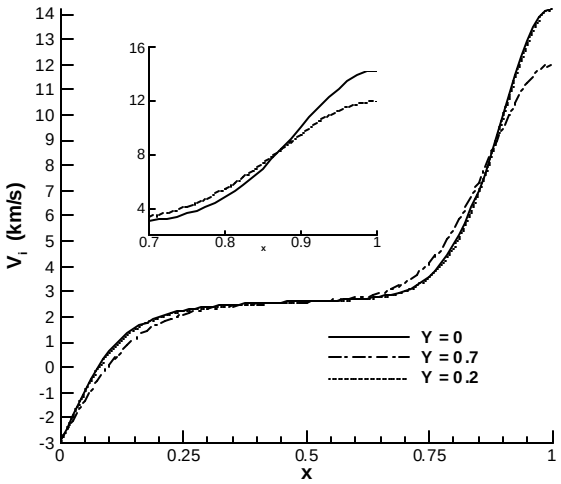

Figure 6b. Ion velocity shows the influence of sputter.

Fig. 6a describes the ion velocity profiles for Y = 0 and δ = 0.0, 0.8, 0.90, 0.95. In the upstream region, near the inlet, ion moves both towards the anode as well as away from it. This is consistent with the known numerical[19] and experimental[20] results. The ion velocity remains almost constant in the diffusion region and then starts increasing in the acceleration region. There is very little affect of SEE on the ion acceleration in the thruster. Since the SEE does not directly affect bulk ions, it is expected that SEE will affect the ion acceleration only near the wall where the recombination of ions with SEE may cause the loss of the "slow" ions. As a result, ion velocity increases with the increase of SEE though the increase is not large. In the inset of Fig. 6a, the near exit ion velocity has been

enlarged to see this increase clearly for different values of SEE.

The isolated effect of sputter yield for $\delta = 0.0$ and Y = 0.0, 0.7 on calculated ion velocity is shown in Fig. 6b. For Y = 0.7, the effect of sputter yield is significant on the ion velocity. In the acceleration region, sputtering causes nearly 8% increase in the ion velocity suggesting the loss of "slow" ions to the wall, whereas in the downstream about the exit it is the "fast" ions which are lost to the wall resulting in over 15% decrease of the bulk ion velocity. It is consistent with the ion number density behavior since, sputter yield causes slight increase in the plasma number density downstream, retaining the flux in the process unchanged.

In Figure 7, we plot the total potential $f = -\int E_z dz + j'$ for δ = 0.0, 0.8, 0.90, 0.95 and Y = 0 which is notably similar to the observed experimental and numerical profiles.[23] The potential distribution is affected by the varying δ. This is due to the presence of the wall potential j' (Eqn. 18). As δ increases, the upstream potential is about 5% higher than in the absence of SEE. However, in the absence of SEE when sputtering yield Y is turned on, there is no significant change in the potential.

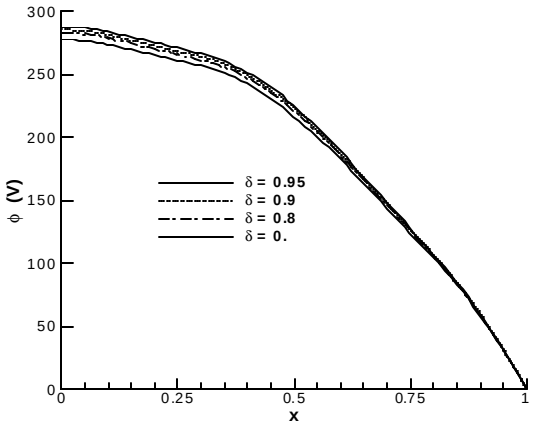

Fig. 7 Potential distribution as a function of δ (SEE).

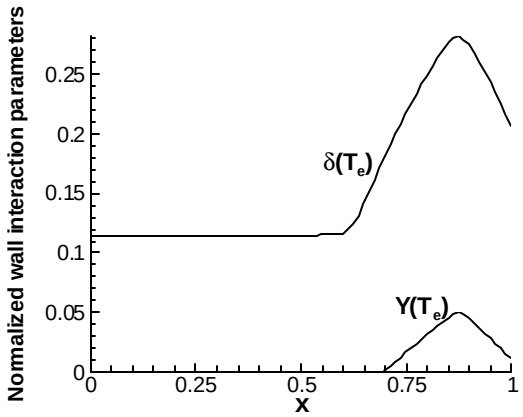

Fig. 8 Distribution of wall interaction parameters along the channel as a function of temperature.

In Figure 8, we plot SEE and sputter yield. We see that since δ (T_e) and Y(T_e) are direct functions of the electron temperature, the curves have peak in the region where electron temperature is maximum. Further, the sputter yield is much smaller than the SEE. Therefore, the effect of SEE is more pronounced on the dynamics than sputter yield. However, for a few thousand hours thruster operation, sputtering will cause the significant erosion of the wall material and the yield Y will increase.

CONCLUSIONS

The analytical model has documented that the plasma-sheath boundary in a plasma without the magnetic field is very sensitive to the secondary electron emission from the wall and the ion sputter yield parameter. In different devices, the plasma sheath has displayed saturation if the coefficient of SEE reaches a threshold value.[6-8] In the presence of ion sputter yield, the sheath potential saturates at lower value of SEE than when SY is absent. The saturation of the wall potential occurs in the presence of ion sputtering. This is due to the fact that in the presence of positive sputtered ions, which condense back on the wall along with the primary ions, the wall potential changes sign sooner than is possible otherwise. The sensitive dependence of wall potential on both SEE and SY is manifested in the energy flux to the wall. In the presence of a constant negative sheath potential, electrons with smaller thermal energies (smaller in comparison with the plasma-sheath potential) will be unable to reach the wall. However, when the wall potential saturates, the wall becomes accessible to all electrons. Therefore, the thermal flux to the wall is enhanced in the presence of both SEE and SY. We note that the upper limit of

SEE and SY is set by the wall potential and the ion energy at the plasma-sheath boundary.

The numerical simulation with the imposed magnetic field has been carried out using the multi-component fluid equation. Owing to the disparate temporal scales of the ions and electrons, ions have been described by the set of time-dependent equations whereas electrons have been described by the steady state equations. The ion velocity profile suggests that due to plasma-wall interaction, most of the "intermediate" energy ions are lost to the wall displaying an "apparent" increase in exit ion velocity for a fixed SEE. The increase in ion velocity is indicative of the loss of the ions to the wall in the presence of SEE. In the absence of SEE and for large sputter yield (Y = 0.7), the ion velocity increases in the acceleration zone and decreases significantly (~15%) near the exit in conformity with the flux conservation. The electron temperature profiles show minor reduction in the presence of SEE, while it slightly increases due to sputter yield. The latter could be due to the loss of slow electrons as they will recombine with the sputtered ions. Further, downstream of the channel half length, the temperature is maximum due to the maximum azimuthal energy near the exit. A small gain (~5%) in potential profile takes place in the presence of SEE. However, sputtering yield does not affect the plasma potential.

ACKNOWLEDGEMENTS

This work is partially supported by NASA GRC research Grant no. NAG3-2520 with David Jacobson as the technical monitor. The second author also recognizes the support of National Academy of Science's NRC fellowship during part of this work.

REFERENCES:

[1]K. U. Riemann, J. Phys. D: Appl. Phys. 24, 493 (1991).

[2]V. A. Godyak and N. Sternberg, Phys. Rev. A 42, 2299 (1990).

[3]N. Sternberg and V. A. Godyak, Physica D, 97, 498 (1996).

[4]J. T. Scheuer and K. C. Walter, {\it Los Alamos National Laboratory report, LA-UR- 94-3920} March 26, (1997).

[5]J. N. Brooks, Phys. Fluids B 2, 1858 (1990).

[6]C. A. Ordonez and R. E. Peterkin Jr., J. App. Phys. 79, 2270 (1996).

[7]L. A. Schwager, W. L. Shu and D. M. Tung, Phys. Fluids B 5, 621 (1993).

[8]L. A. Schwager, Phys. Fluids B 5, 631 (1993).

[9]P. Coakley, N. Hershkowitz, and G. D. Porter, Nucl. Fusion 22, 1321 (1982).

[10]T. Intrator, M. H. Cho, E. Y. Wang, N. Hershkowitz, D. Diebold and J. Decock, J. Appl. Phys. 64, 2927 (1988).

[11]G. D. Hobbs and J. A. Wesson, Plasma Phys. 9, 85 (1967).

[12]S. Roy and B.P. Pandey, J. Plasma Phys., 68, 305 (2002).

[12]M. C. Cross, *Inelastic Ion-Surface Collisions*, Ed. N. H. Tolk, J. C. Tully, W. Heiland, and C. W. White (New York: Academic) p. 253 (1977).

[13]K. F. Stephens and C. A. Ordonez, J. App. Phys. 85, 2522 (1999).

[14]C. A. Ordonez,. Phys. Rev. E 55, 1858 (1997).

[15]J. N. Brooks and D. Naujoks, Phys. Plasmas 7, 2565 (2000).

[16]M. J. Barlow, Mon. Not. R. Astr. Soc. 183, 367 (1978).

[17]Y. Garnier, V. Viel, J.F.Roussel, D.Pagnon, L. Magne and M. Touzeau, IEPC-99-083, Electric propulsion rocket society, 1999.

[18]E. Ahedo, P. Martinez-Cerezo and M. Martinez-Sanchez, in Proceedings of the 37th Joint Propulsion Conference, Salt Lake City, Utah, 2001, AIAA 2001-3323.

[19]E. Ahedo, P. Martinez and M. Martinez-Sanchez, Phys. Plasmas 8, 3058 (2001).

[20]W.A. Hargus Jr. and M.A. Cappelli, J. Propulsion and Power 18, 159 (2002).

[21]S. Roy and B.P. Pandey, Phys. Plasmas 9, 4052 (2002).

[22]R.D. Richtmyer and K.W. Morton, Difference Methods for Initial-Value Problems, 2d ed. (Interscience Publishers, Wiley, New York, 1967).

[23]J. M. Haas and A. D. Gallimore, Phys. Plasmas **8**, 652 (2001).